Author/s:
Christo, SN;Bachhuka, A;Diener, KR;Mierczynska, A;Hayball, JD;Vasilev, K

Title:
The Role of Surface Nanotopography and Chemistry on Primary Neutrophil and Macrophage Cellular Responses

Date:
2016-04-20

Citation:
Christo, S. N., Bachhuka, A., Diener, K. R., Mierczynska, A., Hayball, J. D. & Vasilev, K. (2016). The Role of Surface Nanotopography and Chemistry on Primary Neutrophil and Macrophage Cellular Responses. Advanced Healthcare Materials, 5 (8), pp.956-965. https://doi.org/10.1002/adhm.201500845.

Persistent Link:
https://hdl.handle.net/11343/290900

Article type: Full Paper

The Role of Surface Nanotopography and Chemistry on Primary Neutrophil and Macrophage Cellular Responses

Susan N. Christo[1], Akash Bachhuka[1], Kerrilyn R. Diener, Agnieszka Mierczynska, John D. Hayball[*] and Krasimir Vasilev[*].

S.N.C, Dr K.R.D, A/Prof J.D.H

Experimental Therapeutics Laboratory, Sansom Institute and Hanson Institute, School of Pharmacy and Medical Science, University of South Australia, Adelaide, SA, 5000, Australia
Email: John.Hayball@unisa.edu.au

A.B, A/Prof K.V

Mawson Institute, University of South Australia, Adelaide, SA 5095, Australia
Email: Krasimir.Vasilev@unisa.edu.au

Dr K.R.D, A/Prof J.D.H

This is the author manuscript accepted for publication and has undergone full peer review but has not been through the copyediting, typesetting, pagination and proofreading process, which may lead to differences between this version and the Version of Record. Please cite this article as doi: 10.1002/adhm.201500845.

This article is protected by copyright. All rights reserved.

Research Institute, School of Paediatrics and Reproductive Health, University of Adelaide, Adelaide, SA, 5005, Australia

Dr K.R.D, A/Prof J.D.H

Robinson Research Institute, Discipline of Obstetrics and Gynecology, School of Medicine, University of Adelaide, SA, 5005, Australia

Dr A.M

Australian Wine Research Institute, Adelaide, SA 5064, Australia

A/Prof J.D.H

School of Medicine, University of Adelaide, Adelaide, SA 5005, Australia
Email: John.Hayball@unisa.edu.au

[1]authors contributed equally to this work

Keywords: surface chemistries, surface nanotopographies, neutrophils, macrophages, immunomodulation

This article is protected by copyright. All rights reserved.

Abstract

Synthetic materials employed for enhancing, replacing or restoring biological functionality may be compromised by the host immune responses that they evoke. Surface modification has attracted substantial attention as a tool to modulate the host response to synthetic materials, however, how surface nanotopography combined with chemistry affect immune effector cell responses is still poorly understood. To address this open question we have generated a unique set of model surfaces with controlled surface nanotopography in the range of 16 nm, 38 nm and 68 nm. We also provided tailored outermost surface chemistry that was amine, carboxyl or methyl group rich. The combinations of these properties yielded 12 surface types that are subject to functional assays assessing key immune effector cells, namely primary neutrophil and macrophage responses *in vitro*. Our data demonstrates that surface nanotopography leds to enhanced matrix metalloproteinase-9 production from primary neutrophils, and a decrease in pro-inflammatory cytokine secretion from primary macrophages. Together, these results are the first to directly compare the immunomodulatory effects of the cooperative interplay between surface nanotopography and chemistry.

This article is protected by copyright. All rights reserved.

1. Introduction

Modern medical practice has been increasingly employing synthetic biomaterials to replace or enhance biological tissue functionality. However, the performance of these materials is often compromised by host immune responses. All implanted biomaterials have the potential to induce inflammation, followed by a foreign body response (FBR) and subsequent fibrotic encapsulation.[1, 2] At present, these physiological processes are unpredictable and stochastic.[3] They can lead to pain, discomfort and in some cases rejection of the implanted device. Patients that present with detrimental reactions after surgical implantation receive symptom-specific treatments in an attempt to resolve biological harm. Non-steroidal anti-inflammatory drugs (NSAIDs) are widely prescribed to control inflammation,[4] however, in certain cases such as dental implants, excessive use of NSAIDs may impede bone healing and implant integration, jeopardising the function of the device.[4, 5] This highlights that whilst current 'broad acting' treatments to biomaterial-induced host reactions are effective at short-term reduction of adverse clinical outcomes, there is a need for developing specific approaches to modulating the immune response. Biomaterial device surface modification has been instrumental in improving the integration, functionality and implant biocompatibility by modulating host reactions.[6] Various chemical modification and coatings have been tested with little or no effect. The reason for this is that innate immune cells, such as neutrophils and

This article is protected by copyright. All rights reserved.

macrophages that offer the first line of defence, recognise the foreign body and initiate the processes of inflammation and fibrotic encapsulation.[2, 7]

Recently, surface nanotopography has been identified as an important regulator of cellular and physiological processes.[8] Medical devices come with inherent surface roughness (topography) either intentionally introduced or simply as a result of the manufacturing process. The type, scale and magnitude of surface nanotopography has been demonstrated to affect cell adhesion,[9, 10] density and spreading,[11, 12] cytokine secretion,[13] motility,[14, 15] proliferation and differentiation,[11, 16] and macrophage fusion.[17] For example, Mohuiddin et al. demonstrated a two-fold and three-fold increase in IL-6 secretion by macrophages on 50 nm and 200 nm nanodots respectively, when compared to smooth surfaces. However, the 50nm nanodots also resulted in maximum cell spreading and cell density.[18] In a similar manner, Hulander et al. found that immobilised 56 nm particles decreased platelet activation, whereas the 36 nm particles was advantageous for platelet contact and activation.[10] There are no general rules that apply to how surface nanotopography can affect cell functions because of the disparity between cell types and assays in published reports, as well as differential methods of fabrication of the tested surface. Overall, there are limited published reports on the effect that surface nanotopography has on the functionality of inflammatory cells.[19] Of the ones that are published, outcomes are often contradictory and difficult to

This article is protected by copyright. All rights reserved.

compare due to the different types of surface nanotopography and specific capabilities of a given laboratory. Furthermore, the outermost chemistry of the surfaces used is not purposely tailored and often heterogeneous as a result of the preparation process, which makes the picture even more complex. In view of the importance of inflammatory responses to biomaterials for the rational design of biomedical devices, there is a pressing need to understand how the interplay between surface chemistry and nanotopography affects inflammatory pathways.

In this current study, we aim to bridge this gap of knowledge via an innovative approach using substrata of controlled surface nanotopography on which we could precisely tailor the outermost surface chemistry. These substrata allowed us to interrogate, in a unique manner, the functional responses of primary neutrophils and macrophages; two vital innate immune cells that are the first to interact with an implanted material. We have selected nanotopographies of 16, 38 or 68 nm to address the regime below 100 nm. The outermost surface chemistries involved were amine, methyl and carboxyl rich since these chemistries are consistent with those found in a biological environment.

2. Results and Discussion

This article is protected by copyright. All rights reserved.

2.1 Preparing controllable surface nanotopography and chemistry on planer substrata

To generate controllable surface nanotopography and chemistry we combined plasma polymerisation and electrostatic self-assembly. The schematic of the preparation procedure is presented in **Figure 1**. Model substrata were first modified with a 20 nm thin plasma polymer film deposited from vapour of allylamine. These coatings are known to be rich in amine groups and thus carry a positive charge in aqueous medium at pH < 8.[20] Controlled surface nanotopography was generated by the electrostatic attachment of gold nanoparticles (AuNPs) of nearly monodispersed size of 16, 38 and 68 nm. Gold nanoparticles were selected to generate chemicals from the surface that may interfere with the attaching cells.

As prepared thus far, these substrates present not only a change of nanotopography but also mixed chemistries: an underlying amine/nitrogen rich coating and gold nanoparticles carrying carboxyl acid surface groups. This mixed chemistry is a problem that has been rarely taken into consideration. The problem arises from the inability to discriminate what affects cellular responses – the surface chemistry or nanotopography. We were able to uniquely tailor the outermost surface chemistry by overcoating the attached nanoparticles with a 5 nm thin layer of plasma polymer deposited from vapours of allylamine (AApp), octadiene (ODpp) or acrylic acid (ACpp) which produce films rich in $-NH_2$, $-CH_3$ and –COOH functional groups, respectively (Figure 1). The thickness of the film was selected to ensure preservation of the magnitude of the nanotopography, as well as a continuous

This article is protected by copyright. All rights reserved.

and pinhole free coating.[21] Plasma polymerisation was employed as it is probably the only technique that can generate nanoscale coatings on any type of substrate material.[22]

2D and 3D atomic force microscopy (AFM) images of the modified surface are shown in **Figure 2**A and Figure 2B, respectively. The images confirm effective generation of nanotopography of controlled magnitude and its preservation after overcoating with a 5 nm thin plasma polymer layer. An AFM image of a glass substrate modified with AApp film only, revealing a very smooth surface is also shown. Quantification of these AFM images reveals that the number of immobilised particles decreases with the increase in particle size (Figure 2C); a corresponding increase in surface area when compared to glass control (Figure 2D), and a proportional increase of surface roughness (RMS) with AuNP size (Figure 2E). These parameters were consistent for all surfaces regardless of the type of overcoating (Figure 2G-J). X-ray photoelectron spectroscopy (XPS) was used to determine the chemical composition of the modified surfaces. Table 1 shows that after nanoparticle immobilisation, the gold atomic concentration is 2.3, 3.1 and 4.3 At % for particles sizes of 16 nm, 38 nm and 68 nm, respectively. Several differences are noticeable after overcoating with 5 nm thin plasma polymer films of different chemistries. In all cases, the gold atomic percentage decreases relative to uncoated nanoparticles. This is consistent with the measurement depth of XPS which is ca 10 nm, thus the predominant signal is that AApp based overcoating

This article is protected by copyright. All rights reserved.

provides a nitrogen rich chemistry which leads to increase of the N/C ratio relative to uncoated nanoparticles. At the same time the O/C ratio decreases. The advancing water contact angle (WCA) of the AApp coating without nanotopography is ca 69 degrees and consistent with published studies.[20] As nanotopography is added through the attached nanoparticles, the WCA increases as expected from Wenzel and Cassie theories. The ODpp coating provides a pure hydrocarbon outermost layer, as evidenced by the decrease of both N/C and O/C ratios, with the high WCA further increasing with added nanotopography. ACpp overcoating was used to provide carboxyl acid functionalities, and as expected this is the most hydrophilic surface with the highest O/C ratio. Altogether, the data in Figure 2 and Table 1 demonstrate that we are able not only to generate controlled nanotopography at the nanoscale but also, by utilising plasma polymerisation, uniquely tailor the outermost surface chemistry.

2.2 Modified surface nanotopography modulates neutrophil-derived MMP9 production

Neutrophils are one of the earliest immune cells to contact implanted biomaterials and are recruited to the site from the blood stream. To determine the effect of nanotopography on neutrophils, various activation responses of primary, naïve neutrophils were assessed. As it was important to obtain a resting population of cells for these experiments, neutrophils were

This article is protected by copyright. All rights reserved.

isolated from murine bone marrow by negative selection using a cocktail of antibodies, resulting in a population of greater than 96% pure resting naive Gr-1^{+}CD11b^{+} cells (Figure S1, Supporting Information). These naive neutrophils were incubated on different nanotopographically-modified surfaces and were assessed for surface activation marker expression, namely CD11b (**Figure 3**A) and CD62L (Figure 3B). These receptors are up-regulated and down-regulated, respectively, on activated neutrophils to allow migration from blood vessels into the site of injury.

Neutrophil interactions with invading pathogens results in pathogen engulfment (phagocytosis) and production of reactive oxygen species (ROS) in an attempt to degrade the foreign entity. These short-lived cells then undergo immunologically silent cell death via apoptosis as a mechanism to limit host tissue damage, as well as resolution of inflammation through their clearance by phagocytic cells such as macrophages.[23] Assessment of ROS production (Figure 3C) and the extent of late stage apoptosis (Figure 3D) in neutrophils incubated on different nanotopography modified surfaces reveals no discernible changes in these responses. It was immediately evident that no one particular surface chemical modification, engendered nanotopographical modification, or modification used in combination grossly affects surface activation marker expression, ROS activity or extent of apoptosis. However, further assessment of neutrophil-derived pro-matrix metalloproteinase

This article is protected by copyright. All rights reserved.

(MMP)-9 and the active MMP-9 form was carried out. These key enzymes are involved in tissue remodelling and foreign body responses, including a role in collagen degradation.[24] Interestingly, an increase in neutrophilic MMP-9 (based on the MMP-9 to pro-MMP-9 ratio) is observed on all modified surfaces when compared to glass control surfaces (Figure 3E). Whilst there is minimal variability amongst different AuNP sizes within the AApp and ODpp overcoated groups, the ACpp modified surfaces carrying surface nanotopography displayed a substantial increase in MMP-9, with a two- and three-fold increase in secretion on the 38 nm and 68 nm AuNPs, respectively. This suggests that carboxyl acid rich coatings, when combined with nanotopography, can induce primary neutrophils to secrete a greater level of pro-MMP-9 and MMP-9, without substantially affecting other markers of neutrophil functionality.

2.3 Pro-inflammatory cytokine responses from primary macrophages are diminished on rough and acidic modified surfaces

Another key immune cell that is prominent in the host response to biomaterial implants is macrophages due to their highly plastic phenotype to generate an array of cytokines that skew pro-inflammatory or anti-inflammatory responses. Using *in vitro* cultured primary bone marrow-derived macrophages (BMDM), assessment of how surface nanotopography might influence the functionality of BMDM was carried out by quantifying pro-inflammatory

This article is protected by copyright. All rights reserved.

cytokine release upon activation. The results are presented in Figure 4 and indicate an overall reduction in cytokine expression levels upon the addition of nanotopography for all surface chemical modifications (**Figure 4**A). When compared to both glass control and ACpp without AuNPs, there was a four-fold reduction in TNFα expression by macrophages incubated on 68 nm AuNPs surfaces modified with ACpp (Figure 4A (i)). Levels of IL-6 were decreased on surfaces of 38 nm and 68 AuNPs with AApp and ODpp overcoating, and a similar reduction was observed on 16 nm surfaces modified with ACpp (Figure 4A (ii)). There was a significant drop in IL-6 concentration from 122.7 ng/ml on glass control surfaces to 15.7 ng/ml on 68 nm surfaces modified with ACpp (Figure 4A (ii)). Macrophage secretion of IL-1β exhibited a similar pattern to IL-6 production, whereby IL-1β decreased on nanotopographically modified surfaces of AApp and ODpp overcoating, and the greatest reduction from glass control was observed on nanotopography of 68 nm height modified with ACpp (Figure 4A (iii).

To determine if these cytokine expression levels correlated with cell number, adherent cells were stained with DAPI (Figure 4B), quantified using Image J software, and subsequently represented as cells per surface/coverslip (Figure 4C). Whilst there is an overall reduction in cell numbers for all modified surfaces compared to glass control, there is no significant variability with the addition of nanotopography or surface coatings, suggesting that the

This article is protected by copyright. All rights reserved.

BMDM functionality is in response to the surface nanotopography and not simply a direct effect of cell numbers. The levels of cytokines per cell data is presented in the supporting material in Figure S2. The data trends to support a reduced level of cytokine expression per individual cell when surface nanotopography is added.

In this work we combined plasma polymer deposition with electrostatic self-assembly to generate 12 independent surface types with unique combinations of nanotopography and chemistry for the assessment of primary neutrophil and macrophage responses. Understanding innate immune cell responses to surface modification has important implications on the design and construction of implantable biomaterials. This study quantified functional outputs associated with neutrophil and macrophage activation. When primary neutrophils were exposed to the modified surfaces, there were no observed changes to classical activation responses such as ROS production, CD62L down-regulation or CD11b up-regulation at early time points, nor differences in the degree of apoptosis at a later stage. There were however, gross differences in the production of MMP-9 and pro-MMP-9 whereby all modified surfaces induced an increase in MMP-9 above glass control surfaces. The effect on chemical composition on MMP expression is consistent with published literature but until now has never been interrogated in terms of nanotopography.[25] The MMP proteins are endopeptidases that are constitutively expressed as zymogens and play multiple roles in tissue

This article is protected by copyright. All rights reserved.

remodelling and inflammation upon activation via proteolytic cleavage of their N-terminal pro-peptide.[24] The activation of neutrophils is known to release MMP-9 and the action of this protein has been described in the FBR *in vivo*.[26] However, definitive roles of MMP-9 in the events of the FBR appear to be tissue and biomaterial specific, therefore require further empirical assessment.

There was a nanotopography size-dependent decrease in macrophage secretion of IL-6, IL-1β, and to a lesser extent, TNFα, in particular on ACpp surfaces. These observations are consistent with reports demonstrating hydrophilic -COOH surfaces have reduced leukocyte recruitment, inflammatory responses and fibrotic encapsulation *in vivo*.[6, 27, 28] It has been shown that hydrophilic anionic surfaces increase biomaterial-adherent macrophage apoptosis and reduce macrophage adhesion and fusion at later stages.[29, 30] Studies have also demonstrated that such surfaces can promote a more anti-inflammatory environment by decreasing cytokine levels.[30, 31]

The levels of MMP-9 and TNFα were mostly conserved amongst AuNPs on the hydrophilic amine group rich AApp surfaces, with reductions in IL-6 and IL-1β concentrations observed for increasing surface nanotopography. Such positively charged surfaces have been reported to enhance protein binding in a favourable confirmation, resulting in greater macrophage

This article is protected by copyright. All rights reserved.

interactions and functionality.[32, 33] This was evident in the equivalent or increased cytokine response on AApp surfaces when compared to glass control surfaces. It is important to note that all modified surfaces had equivalent, albeit reduced cell numbers compared to glass control surfaces, confirming that the total number of adherent cells did not account for the functional differences observed.[30] Interestingly, hydrophobic ODpp surfaces revealed similar patterns to AApp surfaces despite the understanding that whilst these surfaces can recruit more leukocytes *in vivo*, proteins appear to adsorb tightly, subsequently inducing undesirable responses, such as enhanced inflammatory signals and increased capsule thickness around the biomaterial.[27, 33, 34] Our data shows that the increase in surface nanotopography was more influential in decreasing IL-6 and IL-1β responses, suggesting a more prominent role of surface nanotopography and that wettability alone cannot be used as a reproducible correlate of cell functionality.[35] It is not surprising that the most dramatic responses were observed on 68 nm AuNPs, considering the nature of cellular interactions with extracellular matrix, which embodies an architecturally complex 3D structure composed of numerous pores, proteins and fibres in the scale of ~60 nm.[11, 14, 36]

3. Conclusion

The greatest challenge in the field of biomaterials is the understanding, and importantly, the prediction of long-term biological responses in patients receiving implantable materials.

This article is protected by copyright. All rights reserved.

Reconstructing and detailing these mechanisms may allow for more targeted approaches, and highlights how immune processes are amenable to manipulation by synthetic biomaterials. In this study, we were able to uniquely fabricate surfaces of controlled and tailored nanotopography and outermost surface chemistry, and interrogate the responses of primary neutrophils and macrophages. We found that nanotopography was capable of reducing MMP-9 expression in neutrophils. In the case of macrophages the levels of expression of IL-6 and IL-1β was reduced by surface nanotopography in the case of all chemical modifications involved. The capacity to effectively modulate neutrophil and macrophage responses through surface nanotopography may translate into favourable outcomes in a clinical setting of biomaterial implantation and may also affect the foreign body response. We anticipate that future explorations in this field of research will facilitate the rational design of biomedical implants with physicochemical surface characteristics tailored at the nanoscale that will enhance utility and function and improve clinical outcomes.

4. Experimental Section

Synthesis of gold nanoparticles

Gold (Au) nanoparticles (NPs) were synthesized by reducing hydrogen tetrachloroaurate (HAuCl4) using trisodium citrate, before a 0.01% HAuCl4 solution was boiled with vigorous stirring. Particles of 16, 38 and 68 nm diameter were synthesised by varying the amount of

This article is protected by copyright. All rights reserved.

1% trisodium citrate from 1 ml to 0.3 mL, respectively,[37] which altered the colour of the solutions from light yellow to wine red. The solution was boiled for an additional 20 mins before being left to cool down to room temperature,[37] and then surface modification of these nanoparticles was performed by using 2-mercaptosuccinic acid as described elsewhere.[38]

Immobilisation of gold nanoparticles

For immobilisation, plasma polymerised allylamine (AApp) samples were immersed in a solution of gold nanoparticles for different time intervals ranging from 2 to 15 hrs depending on the size of particles. These surfaces when immersed in solution carry positive charge while nanoparticles are capped with negatively charged carboxylic acid. This lead to an electrostatic binding between positively charged AApp and negatively charged gold nanoparticles. For our experiments, we immersed AApp in 3 different sized gold nanoparticles (16, 38 and 68 nm). Finally, to remove loosely bound nanoparticles these samples were washed with Milli-Q water and dried using nitrogen.

Plasma polymerisation

Plasma polymerisation was carried out in a custom built reactor with a 13.56 MHz plasma generator.[39] Deposition of allylamine (AA), acrylic acid (AC) and octadiene (OD) was carried out at a pressure of 0.2 mbar and a deposition time of 2 minutes was employed. Power

This article is protected by copyright. All rights reserved.

used for deposition of all three monomers was 40 W, 10 W and 20 W, respectively. Using these conditions a polymer film of thickness 23 nm, 20 nm and 25 nm was obtained, respectively. A film of 5 nm thickness, used for overcoating, was achieved keeping a constant deposition time of 20 secs for all monomers. Before deposition, all substrates were cleaned by applying air plasma for 2 mins at 50 W.

Atomic force microscopy

An NT-MDT NTEGRA SPM atomic force microscope (AFM) was used in non-contact mode to provide nanotopographical images. Au coated silicon nitride tips were used in non-contact mode on the reflective side (NT-MDT, NSG03) and had resonance frequencies between 65 and 100 kHz. Images of 5 μm x 5 μm were scanned at a scan rate of 0.5Hz and amplitude of oscillation of 10nm. Image J was employed for calculating number of particles from these AFM images. The number of particles was used to calculate percentage increase in surface area, percentage surface coverage and interparticle distance. For calculating number of nanoparticles per μm^2, % increase in surface area, % surface coverage, and interparticle distance we have prepared three samples per nanoparticle size. These samples were analyzed by taking three images per sample.

X- ray photoelectron spectroscopy (XPS) analysis

This article is protected by copyright. All rights reserved.

XPS was used to determine the surface composition of the plasma polymers with the deposited AuNPs. Spec SAGE XPS spectrometer equipped with a monochromatic Mg radiation source was operated at 10 kV and 20mA to record all spectra. Survey spectra were recorded at pass energy of 100eV and 0.5eV resolution for identifying the atomic concentrations of all samples. All binding energies (BE) were corrected relative to a neutral C1s carbon peak at 285.0 eV. Processing and curve fitting was performed in Casa XPS.

Animals

All experimental protocols were approved by the Animal Ethics Committees of SA Pathology (Project Number 56.12) and the University of Adelaide (Project Number M-2012-11). All methods were performed in accordance to the guidelines of the University of South Australia (South Australian Animal Welfare Act 1985). Normal C57Bl/6 (B6) mice were bred and housed at the Reid Animal Facility at the University of South Australia. All mice were 8-12 weeks of age, and all experiments were approved by the SA Pathology and University of Adelaide animal ethics committee, and conducted following national and institutional ethical guidelines.

Primary neutrophil purification from bone marrow

This article is protected by copyright. All rights reserved.

Primary resting neutrophils were purified from the bone marrow of mice as previously described.[40] Briefly, bone marrow was flushed from the tibia and femur bones of B6 mice and red blood cells were lysed. Cells were pelleted, and resuspended in 500 µL of PBS before the addition of the negative selection cocktail with the following biotinylated antibodies (per 10^7 cells); anti-CD5 (250 ng), anti-CD45R (125 ng), anti-CD49b (250 ng), anti-CD117 (100 ng), anti-F4/80 (500 ng) and anti-TER 119 (100 ng). All antibodies were purchased from eBioscience.

Antibodies were incubated with cells for 15 mins, rotating at 4°C, washed once, then resuspended in 100 µL MACS buffer per 10^7 cells and 15 µL of anti-biotin microbeads (Miltenyi Biotec) per 10^7 cells for an addition 15 mins (rotating at 4°C). Labelled cells were washed in 10 mL MACS buffer and resuspended in 500 µL MACS buffer. MACS LS Columns (Miltenyi Biotec) were prepared according to manufacturer's instructions before labelled cells were applied to the column 200 µL at a time, followed by three 1 mL MACS buffer washes. The final addition of 100 µL was followed with an additional 3mL wash.

The collected cells were stained with fluorescent antibodies against CD11b and Gr-1 to determine the proportion of neutrophils before (Supplementary Figure 1A) and after (Supplementary Figure 1B) purification. To assess the activation status of the purified

This article is protected by copyright. All rights reserved.

neutrophils, CD62L expression was quantified in unstimulated cells and cells stimulated with 10 ng/mL of PMA for several different time points (Supplementary Figure 1C). All fluorescence values were acquired on the FACSCanto II flow cytometer and analysed using the FlowJo software.

Assessing neutrophil activation by surface marker expression

Purified resting neutrophils ($1x10^6$ cells/mL in PBS) were incubated at 37°C on glass coverslips of various nanotopography and chemical coating placed in wells of a 24-well plate. After 1 hr, neutrophils were immediately cooled on ice before cells were collected by gently scraping off surface and stained with 1 µg/mL anti-CD11b and anti-Gr-1 for 30 mins on ice. Cells were washed twice, and run on the FACS Canto II flow cytometer. FlowJo software was used to analyse the data and calculate mean fluorescence intensity (MFI).

Detecting neutrophil apoptosis

Neutrophils ($1x10^6$ cells/mL in complete RPMI) were plated on glass coverslips of various nanotopography and chemical coatings at 37°C overnight (16 hrs) to allow apoptosis to occur, then immediately cooled on ice before cells were collected by gently scraping off surface. Neutrophils were washed, resuspended in Annexin V binding buffer and stained with 3 µL/sample of Annexin V (BD Biosciences) and 1 µL/sample DAPI (Sigma Aldrich) for 15

This article is protected by copyright. All rights reserved.

mins at room temperature. Samples were immediately run on the FACS Canto II flow cytometer and analysed using FlowJo software.

Determining reactive oxygen species

Plated neutrophils ($1x10^6$/mL cells in PBS) were incubated on glass coverslips of various nanotopography and chemical coatings at 37°C for 30 mins, immediately cooled on ice, and cells were collected by gently scraping off surface. Neutrophils were washed, and resuspended in 500 µL PBS containing 1 mM CM-H2DCFDA (prepared according to manufacturer instructions, Life Technologies) and 1 µg/mL anti-Gr-1, for 20 mins at room temperature. Cells were washed, and samples were immediately run on the FACS Canto II flow cytometer for analysis using FlowJo software.

Quantifying MMP-9 production by gelatin zymography

Neutrophils ($1x10^6$ cells/mL in incomplete RPMI/surface) were plated on glass coverslips of various nanotopography and chemical coatings at 37°C for 16 hrs. Supernatant was collected, concentrated and buffer was exchanged on a 10MWCO spin column (Merck Millipore) according to manufacturer's instructions. A total of 1 µg of protein was prepared in 2x non-reducing Laemmli buffer before being loaded onto a 10% SDS-PAGE gel containing 1mg/mL of gelatin and resolved via electrophoresis. The resultant gel was washed twice in

This article is protected by copyright. All rights reserved.

renaturing buffer (2.5% Triton-X in MQ water) and once in developing buffer (50 nM Tris-HCl, 5 mM CaCl2 and 0.02% NaN3 in MQ water, pH 7.4). Fresh developing buffer was added and incubated at 37°C for 24 hrs. All washes were performed with gentle shaking (60 rpm) for 30 mins unless otherwise indicated.

The developed gels were stained with coomassie blue stain, followed by destaining gels with destain buffer (water, methanol, and acetic acid in a ratio of 50:40:10 v/v/v) to detect clear bands indicative of digested gelatine due to the presence of pro-MMP-9 (~92 kDa) and MMP-9 (~82 kDa). Images of gels were scanned and semi-quantified using ImageJ density function. Zymographs are ideal in this situation because it allowed both MMP-9 and pro-MMP-9 to be detected and plotted as a ratio.

Preparing L929 conditioning media

To prepare L929 conditioned media, confluent L929 cells were detached, collected and passaged 1:10. Cells were then cultured until the media was exhausted (7-8 days). The conditioned media, which contained the macrophage growth factor M-CSF, was removed, filtered (0.22 µm), aliquoted and stored at -20°C until required.

In vitro culture of bone marrow derived macrophages

This article is protected by copyright. All rights reserved.

Bone marrow derived macrophage (BMDM) cells were generated by flushing bone marrow cells from femurs and tibia of B6 mice, depleting red blood cells using lysis buffer, and resuspending cell in complete RPMI supplemented with 20% L929 conditioned media. On day 4 of culture, suspension cells were removed, and media replenished before being seeded ($0.5x10^6$ cells/well in 500 uL) on coverslips modified with the indicated surface nanotopography. Cells were maintained for an additional three days at 37°C/5%C02 to allow for full differentiation into macrophages. To assess BMDM phenotype, cells were gently scraped off on day 7 of culture and stained with anti-CD11b and anti-F4-80 antibodies for 30 mins on ice. Cells were washed, fixed and later ran on the flow cytometer for detection of CD11b+F4-80+ events using the FlowJo software. This method allowed bound monocytes to differentiate into macrophages on the various surfaces for three days before external stimuli were added to assess how surface interactions influenced known macrophage function.

Cytokine secretion from activated macrophages

On day 7, the in vitro generated BMDMs were stimulated with lipopolysaccharide (LPS, serotype O111:B4; 100 ng/mL; Sigma Aldrich) or left unstimulated for 4 hrs, and supernatant collected for the analysis of TNF-α, and IL-6. There was no IL-10 detected in these cultures (data not shown). BMDMs were then stimulated with adenosine triphosphate (ATP, 5 mM;

This article is protected by copyright. All rights reserved.

Sigma Aldrich) for 1 hr, and supernatant collected for IL-1β analysis using standard ELISA protocols. Cytokines were not detected in unstimulated cultures (data not shown).

Quantifying numbers of adherent bone marrow derived macrophages

BMDM plated onto surfaces were gently washed with PBS before fixing with 100% methanol overnight. Cells were stained with 1 µg/mL DAPI for 2 mins at room temperature, and washed twice before mounting onto glass slide. Four images per surface were taken using an Olympus IX51 Fluorescence Microscope and the CellSens program. ImageJ software was used to automatically count the cells in the field of view, and the image dimensions (in µm) were used to calculate total cell numbers on the total area of the 13 mm-diameter glass coverslip.

Statistical Analysis

All statistical analysis was performed on GraphPad Prism 5, and a one-way analysis of variance (ANOVA) performed with a Dunnett's posttest. Each surface nanotopography was compared against the glass surfaces, which was selected as the control.

Supporting Information

Supporting Information is available from the Wiley Online Library or from J.D.H and K.V.

This article is protected by copyright. All rights reserved.

Acknowledgements

This project was support in part by project grants NHMRC PG631931 and ARC DP15104212 (both to J.D.H and K.V). S.N.C and A.B contributed equally to this work. Equal corresponding authors are J.D.H and K.V.

Received: ((will be filled in by the editorial staff))
Revised: ((will be filled in by the editorial staff))
Published online: ((will be filled in by the editorial staff))

This article is protected by copyright. All rights reserved.

References

[1] J. M. Anderson, A. Rodriguez, D. T. Chang, *Semin Immunol* **2008**, *20*, 86.

[2] S. Franz, S. Rammelt, D. Scharnweber, J. C. Simon, *Biomaterials* **2011**, *32*, 6692.

[3] W. Kenneth Ward, *J Diabetes Sci Technol* **2008**, *2*, 768.

[4] D. G. Kalyvas, M. Tarenidou, *J Oral Sci* **2008**, *50*, 239.

[5] B. Winnett, H. C. Tenenbaum, B. Ganss, A. Jokstad, *Clin Oral Implants Res* **2014**.

[6] S. Kamath, D. Bhattacharyya, C. Padukudru, R. B. Timmons, L. Tang, *J Biomed Mater Res A* **2008**, *86*, 617.

[7] L. Mesure, G. De Visscher, I. Vranken, A. Lebacq, W. Flameng, *PLoS One* **2010**, *5*, e12949.

[8] H. M. Rostam, S. Signgh, N. E. Vrana, M. R. Alexander, A. M. Ghaemmaghami, *Biomater. Sci.* **2015**, *3*, 424.

[9] J. R. Gamboa, S. Mohandes, P. L. Tran, M. J. Slepian, J. Y. Yoon, *Colloids Surf B Biointerfaces* **2013**, *104*, 318; J. Fink, R. Fuhrmann, T. Scharnweber, R. P. Franke, *Clin Hemorheol Microcirc* **2008**, *39*, 205.

[10] M. Hulander, A. Lundgren, L. Faxalv, T. L. Lindahl, A. Palmquist, M. Berglin, H. Elwing, *Colloids Surf B Biointerfaces* **2013**, *110*, 261.

[11] V. Vogel, M. Sheetz, *Nat Rev Mol Cell Biol* **2006**, *7*, 265.

[12] C. L. Gilchrist, D. S. Ruch, D. Little, F. Guilak, *Biomaterials* **2014**, *35*, 10015.

[13] Q. L. Ma, L. Z. Zhao, R. R. Liu, B. Q. Jin, W. Song, Y. Wang, Y. S. Zhang, L. H. Chen, Y. M. Zhang, *Biomaterials* **2014**, *35*, 9853; K. S. Tan, L. Qian, R. Rosado, P. M. Flood, L. F. Cooper, *Biomaterials* **2006**, *27*, 5170.

[14] E. K. Yim, R. M. Reano, S. W. Pang, A. F. Yee, C. S. Chen, K. W. Leong, *Biomaterials* **2005**, *26*, 5405.

[15] J. M. Lopacinska, C. Gradinaru, R. Wierzbicki, C. Kobler, M. S. Schmidt, M. T. Madsen, M. Skolimowski, M. Dufva, H. Flyvbjerg, K. Molhave, *Nanoscale* **2012**, *4*, 3739.

[16] R. A. Gittens, T. McLachlan, R. Olivares-Navarrete, Y. Cai, S. Berner, R. Tannenbaum, Z. Schwartz, K. H. Sandhage, B. D. Boyan, *Biomaterials* **2011**, *32*, 3395.

[17] S. Chen, J. A. Jones, Y. Xu, H. Y. Low, J. M. Anderson, K. W. Leong, *Biomaterials* **2010**, *31*, 3479.

[18] M. Mohiuddin, H. A. Pan, Y. C. Hung, G. S. Huang, *Nanoscale Res Lett* **2012**, *7*, 394.

[19] S. Svensson, M. Forsberg, M. Hulander, F. Vazirisani, A. Palmquist, J. Lausmaa, P. Thomsen, M. Trobos, *Int J Nanomedicine* **2014**, *9*, 775; T. D. Zaveri, N. V. Dolgova, B. H. Chu, J. Lee, J. Wong, T. P. Lele, F. Ren, B. G. Keselowsky, *Biomaterials* **2010**, *31*, 2999.

[20] A. Mierczynska, A. Michelmore, A. Tripathi, R. V. Goreham, R. Sedev, K. Vasilev, *Soft Matter* **2012**, *8*, 8399.

[21] A. Michelmore, P. Martinek, V. Sah, R. D. Short, K. Vasilev, *Plasma Process Polym* **2011**, *8*, 367; R. V. Goreham, A. Mierczynska, M. Pierce, R. D. Short, S. Taheri, A. Bachhuka, A. Cavallaro, L. E. Smith, K. Vasilev, *Thin Solid Films* **2013**, *528*, 106.

[22] K. Vasilev, A. Michelmore, H. J. Griesser, R. D. Short, *Chem Commun (Camb)* **2009**, 3600; K. Vasilev, A. Michelmore, P. Martinek, J. Chan, V. Sah, H. J. Griesser, R. D. Short, *Plasma Process Polym* **2010**, *7*, 824.

[23] S. Fox, A. E. Leitch, R. Duffin, C. Haslett, A. G. Rossi, *J Innate Immun* **2010**, *2*, 216.

[24] D. T. Luttikhuizen, M. J. van Amerongen, P. C. de Feijter, A. H. Petersen, M. C. Harmsen, M. J. van Luyn, *Biomaterials* **2006**, *27*, 5763.

[25] J. A. Jones, A. K. McNally, D. T. Chang, L. A. Qin, H. Meyerson, E. Colton, I. L. Kwon, T. Matsuda, J. M. Anderson, *J Biomed Mater Res A* **2008**, *84*, 158.

[26] W. Tian, T. R. Kyriakides, *Matrix Biol* **2009**, *28*, 148.

[27] J. N. Barbosa, P. Madureira, M. A. Barbosa, A. P. Aguas, *J Biomed Mater Res A* **2006**, *76*, 737.

[28] A. Nair, L. Zou, D. Bhattacharyya, R. B. Timmons, L. Tang, *Langmuir* **2008**, *24*, 2015.

This article is protected by copyright. All rights reserved.

[29] W. G. Brodbeck, M. S. Shive, E. Colton, Y. Nakayama, T. Matsuda, J. M. Anderson, *J Biomed Mater Res* **2001**, *55*, 661.

[30] J. M. Anderson, J. A. Jones, *Biomaterials* **2007**, *28*, 5114.

[31] W. G. Brodbeck, Y. Nakayama, T. Matsuda, E. Colton, N. P. Ziats, J. M. Anderson, *Cytokine* **2002**, *18*, 311.

[32] P. Thevenot, W. Hu, L. Tang, *Curr Top Med Chem* **2008**, *8*, 270; B. G. Keselowsky, D. M. Collard, A. J. Garcia, *J Biomed Mater Res A* **2003**, *66*, 247.

[33] B. G. Keselowsky, D. M. Collard, A. J. Garcia, *Biomaterials* **2004**, *25*, 5947.

[34] P. Rico, J. C. Rodriguez Hernandez, D. Moratal, G. Altankov, M. Monleon Pradas, M. Salmeron-Sanchez, *Tissue Eng Part A* **2009**, *15*, 3271.

[35] B. Cortese, M. O. Riehle, S. D'Amone, G. Gigli, *J Colloid Interface Sci* **2013**, *394*, 582.

[36] K. R. Kam, L. A. Walsh, S. M. Bock, J. D. Ollerenshaw, R. F. Ross, T. A. Desai, *Tissue Eng Part A* **2014**, *20*, 130.

[37] J. Turkevich, P. C. Stevenson, J. Hillier, *Discussions of the Faraday Society* **1951**, *11*, 55.

[38] T. Zhu, K. Vasilev, M. Kreiter, S. Mittler, W. Knoll, *Langmuir* **2003**, *19*, 9518.

[39] K. Vasilev, A. Michelmore, P. Martinek, J. Chan, V. Sah, H. J. Griesser, R. D. Short, *Plasma Processes and Polymers* **2010**, *7*, 824.

[40] M. Hasenberg, A. Kohler, S. Bonifatius, K. Borucki, M. Riek-Burchardt, J. Achilles, L. Mann, K. Baumgart, B. Schraven, M. Gunzer, *PLoS One* **2011**, *6*, e17314.

This article is protected by copyright. All rights reserved.

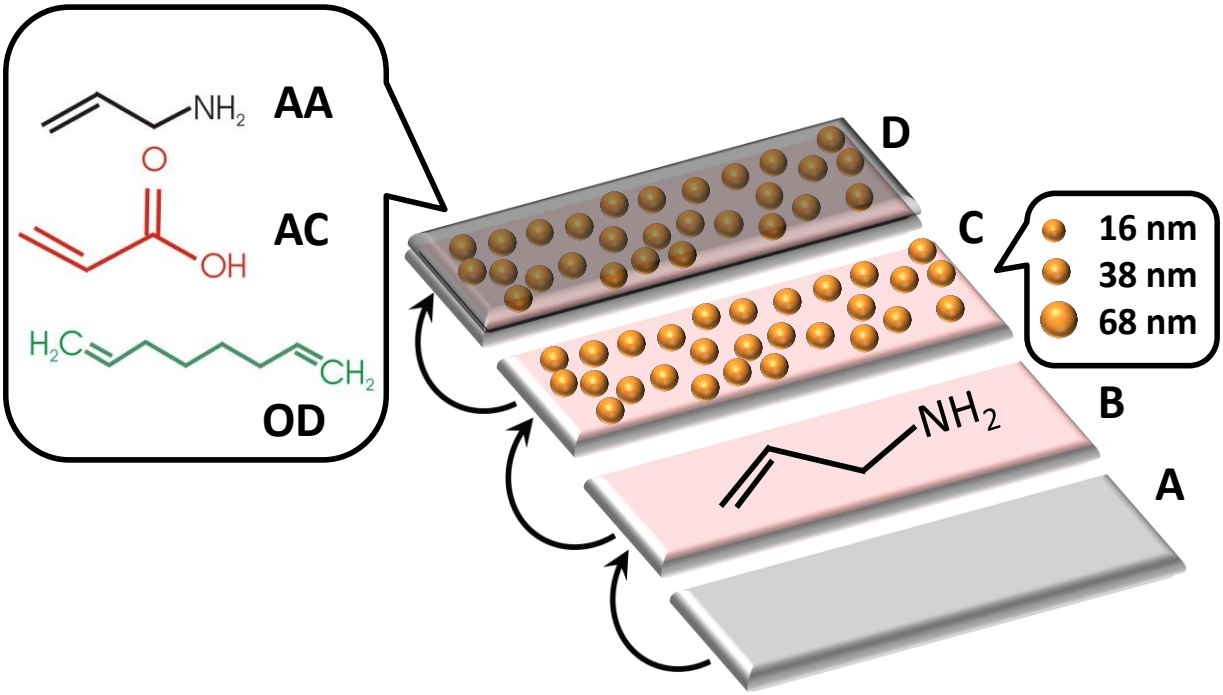

Figure 1. Schematic diagram representing the process of generating different nanotopography modified surfaces. Plasma polymerisation was used to coat (A) glass coverslips with (B) a plasma polymer film deposited from vapour of allylamine, followed by (C) immobilization of gold nanoparticles (16, 38 and 68nm) and (D) overcoating with a 5 nm thin plasma polymer film deposited from vapour of allylamine (AApp), acrylic acid (ACpp) or octadiene (ODpp).

This article is protected by copyright. All rights reserved.

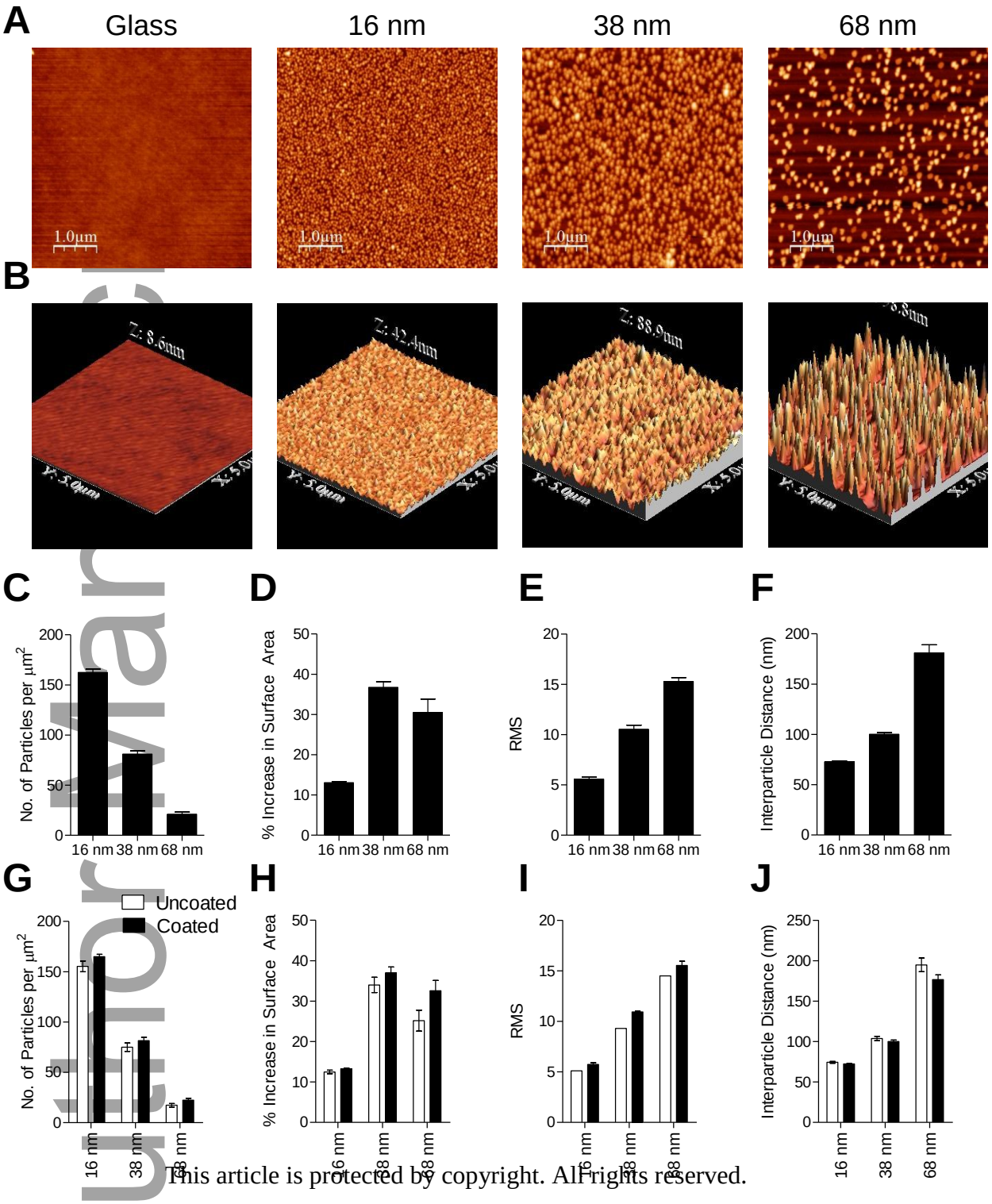

Figure 2. Atomic Force Microscopic analysis of surfaces modified with 16, 38 or 68 nm gold nanoparticles and overcoated with a 5 nm thin layer of AApp in (A) two, and (B) three dimensions. The (C) number of particles, (D) percentage increase in surface area, (E) roughness based on root mean squared (RMS), and (F) interparticle distance, were calculated for 16, 38 and 68 nm. Surfaces that were uncoated (white bars) or coated (black bars) with different surface chemistry were assessed for (G) number of particles, (H) percentage increase in surface area, (I) RMS, and (J) interparticle distance. Scale bar in (A) 1 µm, and (B) 5 µm x 5 µm on the X and Y axis.

This article is protected by copyright. All rights reserved.

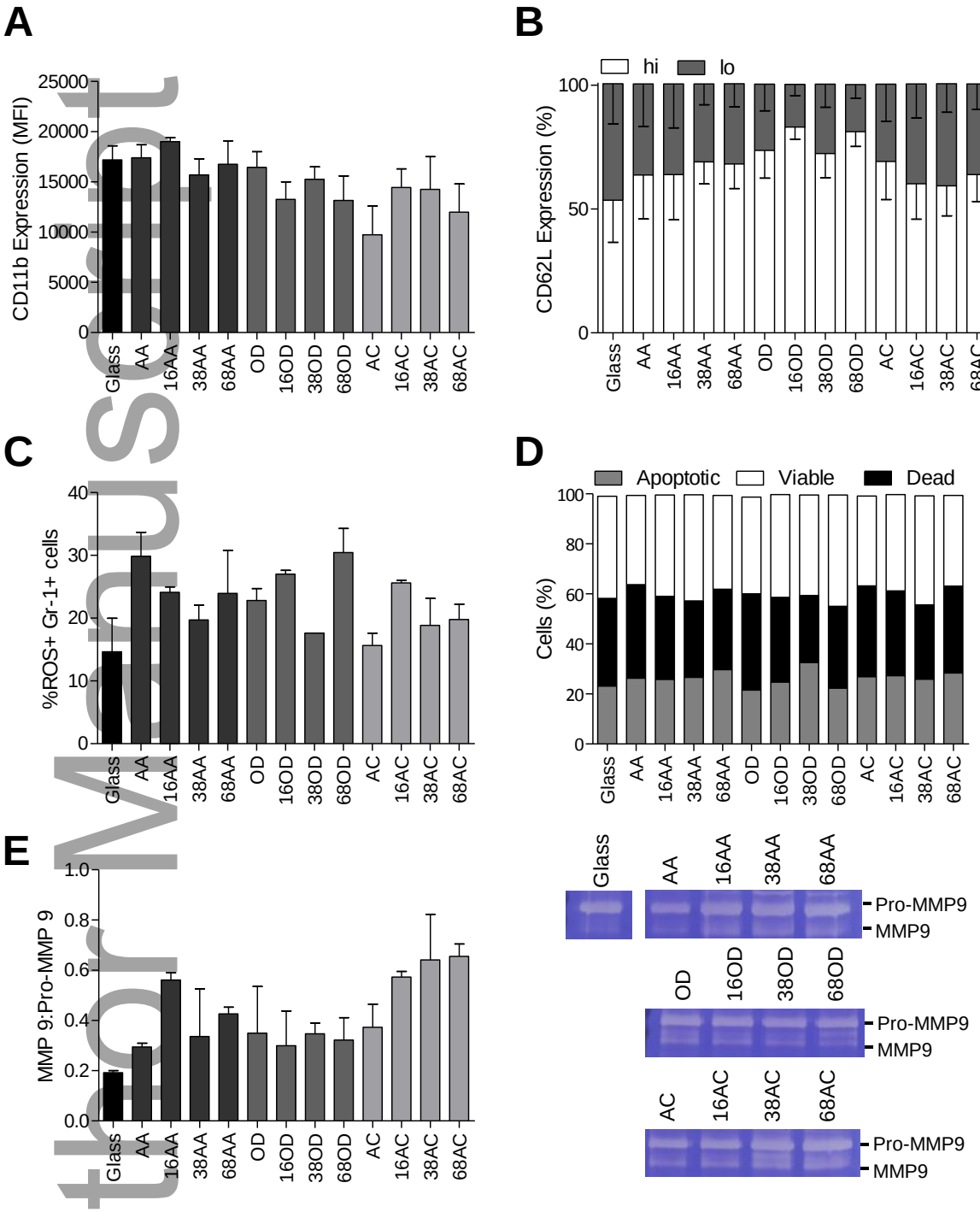

This article is protected by copyright. All rights reserved.

Figure 3. Early activation responses of primary neutrophils are not altered on different nanotopography modified surfaces but MMP-9 production is enhanced on rough and acidic surface modifications. Purified naïve neutrophils were purified from bone marrow and incubated on the surfaces for the assessment of (A) CD11b expression, and (B) percentage of $ROS^{+}Gr\text{-}1^{+}$ cells. (C) The activation marker CD62L marker is also quantified based on hi and lo expression. (D) Neutrophil apoptosis and cell death are detected using standard DAPI and Annexin-V staining methods. (E) Neutrophils are incubated on the surfaces for 16 hrs before supernatant is collected, concentrated and the buffer was exchanged on a 10MWCO spin column. A total of 1 ug protein was run for the detection of pro-MMP-9 (~92 kDa) and MMP-9 (~82 kDa) by gelatin zymography. Results are representative of two to three independent experiments, and data shown as mean ± SEM. The p values were calculated in reference to the control glass surface and were not significant against nanotopography surfaces as deduced via one-way analysis of variance with the Dunnett's post-test.

This article is protected by copyright. All rights reserved.

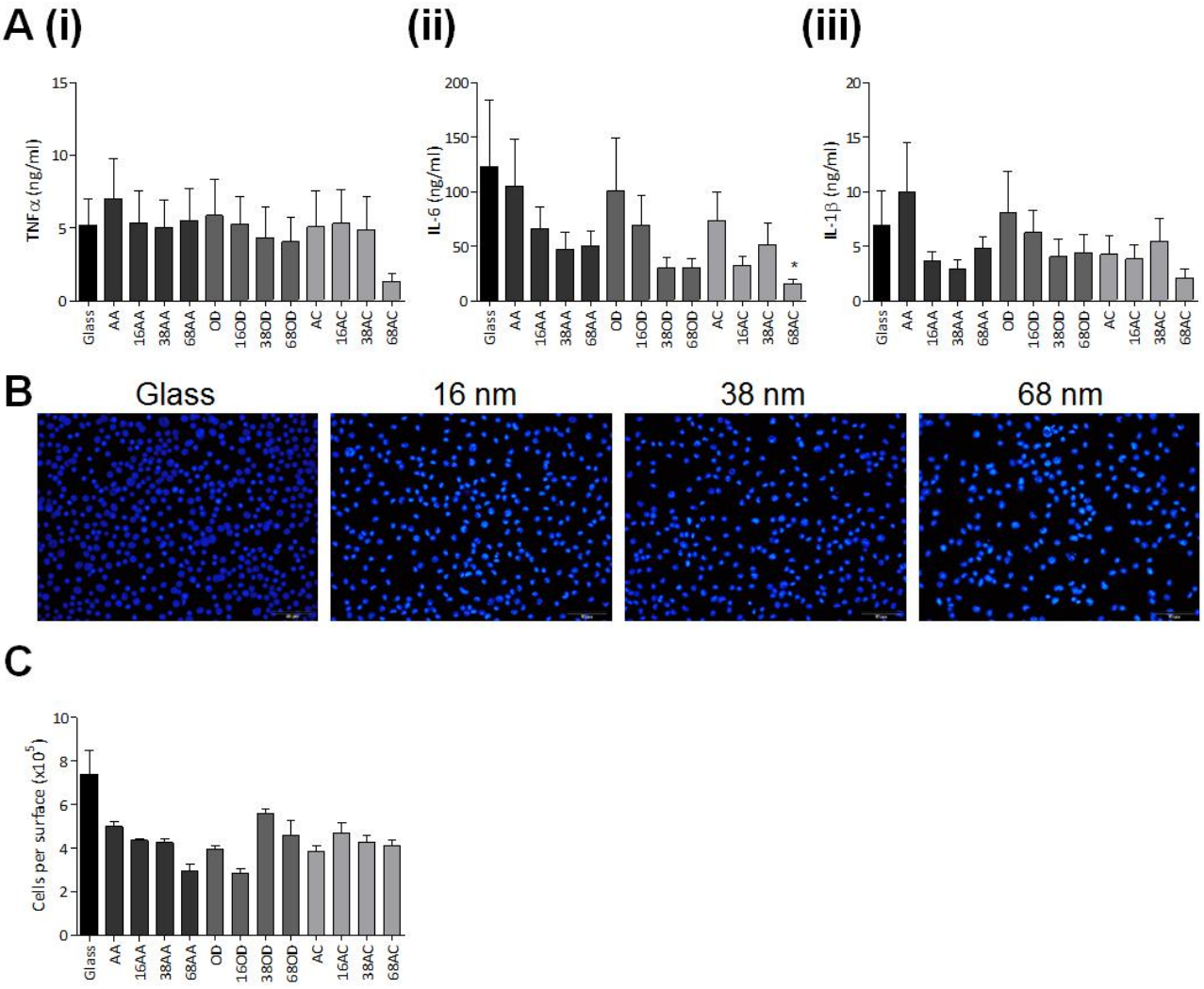

Figure 4. Secretion of pro-inflammatory cytokines by primary macrophages is reduced on rough and acidic modified surfaces. Bone marrow-derived macrophages were cultured and plated on different nanotopography modified surfaces prior to stimulation with 100 ng/ml LPS for the detection of TNFα (A (i)) and IL-6 cytokines (A (ii)). Secondary 5 mM ATP stimulation was performed prior to measuring IL-1β (A (iii)) secretion using standard ELISA. BMDM incubated on the surfaces are fixed and stained with DAPI for microscopic detection (B) and quantification of cell adhesion numbers using the Image

This article is protected by copyright. All rights reserved.

J software (C). Representative images in (B) are taken from AApp modified surfaces. Results are representative of three independent experiments, and data shown as mean ± SEM. The p values were calculated in reference to the control glass surface and are denoted as thus: * P<0.05 deduced via one-way analysis of variance with the Dunnett's post-test.

This article is protected by copyright. All rights reserved.

Table 1. Surface chemical composition of different nanotopography modified surface derived from the XPS analysis as well as the corresponding advancing water contact angle (WCA). All the XPS data was plotted with a standard error of 5%.

Surface	Au (At %)	Au/C	N/C	O/C	WCA (degree)
16 nm	2.3	0.03	0.11	0.25	44± 2.2
38 nm	3.1	0.04	0.12	0.2	38± 1.9
68 nm	4.3	0.06	0.16	0.18	57± 2.9
AA	-	-	0.21	0.11	69± 3.5
16AA	1.5	0.02	0.18	0.18	81± 4.1
38AA	1.4	0.02	0.18	0.19	80± 4.0
68AA	1.4	0.02	0.18	0.18	77± 3.9
OD	-	-	-	0.14	95± 4.8
16OD	1.8	0.02	0.03	0.15	117± 5.9
38OD	1.9	0.02	0.03	0.16	114± 5.7
68OD	1.4	0.02	0.02	0.13	103± 5.2
AC	-	-	-	0.31	51± 2.6
16AC	1.5	0.02	0.09	0.29	63± 3.2
38AC	0.9	0.01	0.05	0.29	58± 2.9
68AC	1.2	0.02	0.08	0.29	56± 2.8

This article is protected by copyright. All rights reserved.

Innate immune effector cells can differentially respond to the controlled surface nanotopography in the range of 16 nm, 38 nm and 68 nm. Additonal overcoating of these surfaces with amine, carboxyl or methyl group rich chemistries demonstrated that surfaces with hydrophillic anionic overcoated 68 nm gold nanoparticles could modulate neutrophil and macrophage functionality.

Keywords: surface chemistries, surface nanotopographies, neutrophils, macrophages, immunomodulation

S.N.C, A.B, K.R.D, A.M, J.D.H*, K.V*

The Role of Surface Nanotopography and Chemistry on Primary Neutrophil and Macrophage Cellular Responses

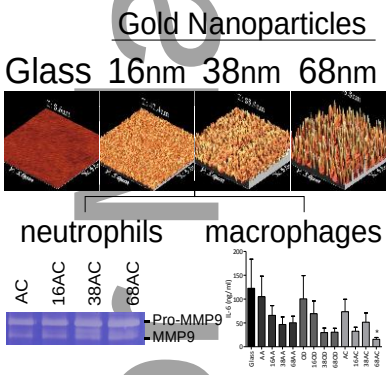

This article is protected by copyright. All rights reserved.

Supporting Information

The role of surface nanotopography and chemistry on primary neutrophil and macrophage cellular responses

Susan N. Christo[1], Akash Bachhuka[1], Kerrilyn R. Diener, Agnieszka Mierczynska, John D. Hayball[*] and Krasimir Vasilev[*].

This article is protected by copyright. All rights reserved.

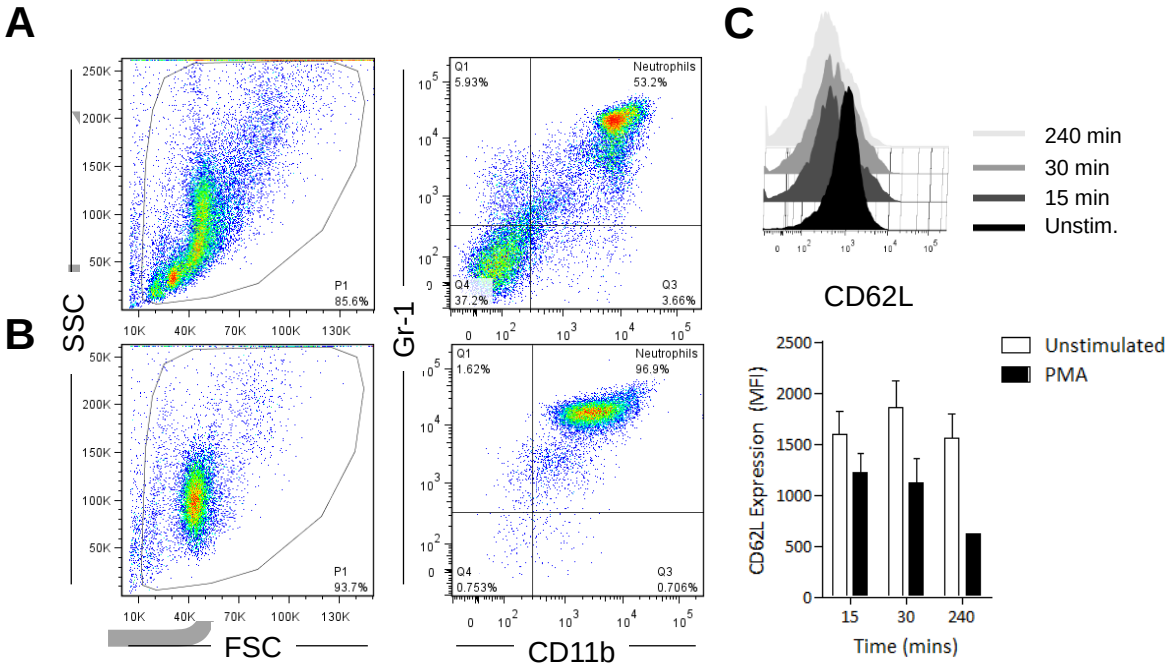

Figure S1. Purification of bone marrow cells for obtaining resting primary neutrophils. Primary neutrophils were negatively selected from bone marrow of mice using biotinylated antibodies against CD5, CD45R, CD49b, F4/80 and Ter119. Cells were incubated with anti-biotin MACS beads and ran on a MACS column as per standard protocol. Unpurified (A) and neutrophil purified (B) neutrophils were stained for CD11b and Gr-1 markers for quantification of double-positive neutrophil purity using flow cytometry. Left panels indicate size (FCS) and complexity (SSC) of cells, with right panels showing expression of Gr-1 and CD11b. (C) The activation status of purified neutrophils was assessed by quantifying the down-regulation of mean CD62L fluorescence. Neutrophils were stimulated with PMA for the indicated time before being cooled on ice, gently scraped off surfaces, and stained for CD62L expression quantified as mean fluorescence intensity (MFI) for assessing resting or activation status.

This article is protected by copyright. All rights reserved.

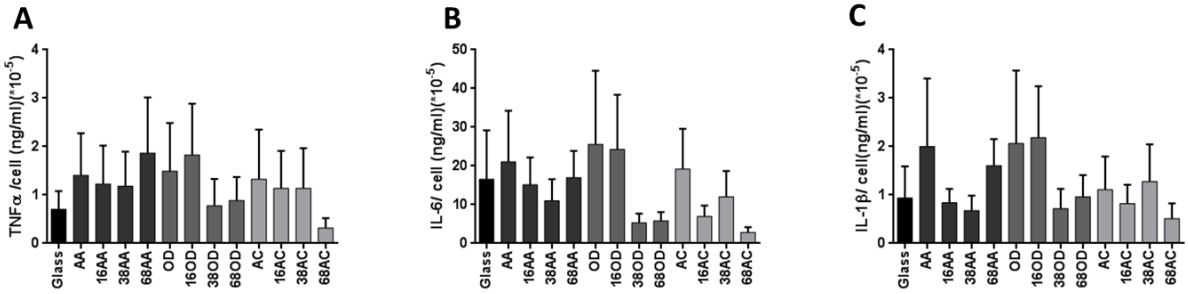

Figure S2. Bone marrow-derived macrophages were cultured and plated on different nanotopography modified surfaces prior to stimulation with 100 ng/ml LPS for the detection of the cytokines TNFα (A) and IL-6 (B). Secondary 5mM ATP stimulation was performed prior to measuring IL-1β secretion (C) using standard ELISA. Results are depicted as cytokine concentration per cell, and are representative of three independent experiments with data shown as mean ± SEM. The p values were calculated in reference to the control glass surface and are denoted as thus: * P<0.05 deduced via one-way analysis of variance with the Dunnett's test.

This article is protected by copyright. All rights reserved.